journal of the mechanical behavior of biomedical materials 158 (2024) 106675

Contents lists available at ScienceDirect

Journal of the Mechanical Behavior of Biomedical Materials

journal homepage: www.elsevier.com/locate/jmbbm

Visible light photo-crosslinking of biomimetic gelatin-hyaluronic acid hydrogels for adipose tissue engineering

Matteo Pitton [a,1], Christian Urzì [a,1], Silvia Farè [a,b,*], Nicola Contessi Negrini [a]

[a] Department of Chemistry, Materials and Chemical Engineering, Politecnico di Milano, Italy
[b] National Interuniversity Consortium of Materials Science and Technology, Florence, Italy

ARTICLE INFO

Keywords:
Adipose tissue engineering
Lipid accumulation
Gelatin
Hyaluronic acid
In vitro model
Hydrogel

ABSTRACT

Tissue engineering (TE) of adipose tissue (AT) is a promising strategy that can provide 3D constructs to be used for *in vitro* modelling, overcoming the limitations of 2D cell cultures by closely replicating the complex breast tissue extracellular matrix (ECM), cell-cell, and cell-ECM interactions. However, the challenge in developing 3D constructs of AT resides in designing artificial matrices that can mimic the structural properties of native AT and support adipocytes biological functions. Herein, we developed photocrosslinkable hydrogels by employing gelatin methacrylate (GelMA) and hyaluronic acid methacrylate (HAMA) to mimic the collagenous and glycosaminoglycan components of AT microenvironment, respectively. The physico-mechanical properties of the hydrogels were tuned to target AT biomimetic properties by varying the hydrogel formulation (with or without hyaluronic acid), and the amount of photoinitiator (ruthenium/sodium persulfate) used to crosslink the hydrogels via visible light. The physical and mechanical properties of the developed hydrogels were tuned by varying the material formulation and the photoinitiator concentration. Preadipocytes were encapsulated inside the hydrogels and differentiated into mature adipocytes. Findings enlightened that HAMA addition in hybrid hydrogels boosted an increased lipid accumulation. The engineered biomimetic adipocyte-based constructs resulted promising as scaffolds or 3D *in vitro* models of AT.

1. Introduction

Adipose tissue (AT) is a highly complex and dynamic connective tissue, essential for homeostasis maintenance through its main functions, as energy storage control, nutrients exchanges regulation, temperature monitoring, and wound healing (Di Stefano et al., 2019; Kothari et al., 2020). AT is located in several anatomical districts, such as subcutaneous and visceral depots. Cellular portion mainly comprises adipocytes with a basement membrane (100 nm), composed of type IV collagen, which represents the major collagenous component of the adipocytic extracellular matrix (ECM) (Freedman and Mooney, 2019). Additionally, other fibrillar collagens (type I, III, V, VI), fibronectin, and a small amount of laminin build the proteinaceous part of adipose ECM, providing dissipation of external stresses. Beside collagens, hyaluronic acid (HA) participates in homeostasis maintenance regulating water exchanges in the adipocytic microenvironment (Ruiz-Ojeda and Aguilera, 2019). During human development, ECM guides cells behavior, functionality, structural arrangement, and migration by activating intracellular pathways (Walker et al., 2018). However, homeostasis alterations typical of pathologies insurgence induce dysregulations in ECM components and alter cell behavior. For example, in breast AT tumors, disease occurrence triggers the increased production of collagens (type I, III, V, VI) and HA around tumor cells or within tumor stroma (Sonbol, 2018; Wang et al., 2018; Xu et al., 2019).

Nowadays, there is an urgent need to understand the role of the ECM components in homeostasis maintenance in adipose tissue. For this reason, 3D modelling has allowed to build complex structures that resemble cell-cell and cell-ECM interactions of native microenvironment (Avtanski et al., 2023). Moreover, designing a 3D model which recapitulates major aspects of tumor insurgence and typical tumor-cells interactions has provided promising 3D platforms to test new therapies and investigate mechanisms of drugs resistance (Bahcecioglu et al., 2020). For adipose TE, 3D models allow the investigation of adipogenesis, adipocyte metabolism, obesity, obesity-related disease, and breast cancer insurgence (Avtanski et al., 2023). Scaffold-free spheroids faithfully resemble *in vitro* the cellular processes related to *in vivo*

* Corresponding author. Department of Chemistry, Materials and Chemical Engineering, Politecnico di Milano, Italy.
E-mail address: silvia.fare@polimi.it (S. Farè).
[1] These authors equally contributed.

https://doi.org/10.1016/j.jmbbm.2024.106675
Received 26 August 2023; Received in revised form 23 April 2024; Accepted 24 July 2024
Available online 25 July 2024
1751-6161/© 2024 The Authors. Published by Elsevier Ltd. This is an open access article under the CC BY-NC-ND license (http://creativecommons.org/licenses/by-nc-nd/4.0/).

adipogenesis, with the possibility to provide insights into mechanisms typical of obesity, breast cancer and adipose inflammation state (Domingues et al., 2023; Horder et al., 2021; Li et al., 2022; Paré et al., 2020). Additionally, recent advantages in organ-on-a-chip technology have enabled the development of micro-physiological systems for drug testing (Flont et al., 2023; Huerta-Reyes and Aguilar-Rojas, 2021; Lugo-Cintrón et al., 2020). However, the absence of a surrounding microenvironment in these *in vitro* models does not allow to recapitulate cell-ECM interactions, limiting their translational potential.

In this context, hydrogels have gained tremendous attention for adipose TE, since they provide biological cues for cell adhesion and absorb huge quantities of water and biological fluids (Teixeira and Martins, 2023). Moreover, their features can be finely tailored to better mimic native adipocytic ECM. Natural biomaterials used for mimicking AT are usually components of the native adipose ECM, such as collagen (Chuang et al., 2018; Di Caprio and Bellas, 2020; Hammel and Bellas, 2020; Li et al., 2024; Ni et al., 2023) and hyaluronic acid (Ghaffari-bohlouli et al., 2023; Louis et al., 2017). Alternatively, biomaterials with molecular properties similar to those of AT microenvironment have been involved, such as gelatin (Contessi Negrini et al., 2019a, 2019b, 2020; Tytgat et al., 2019; Van Damme et al., 2021), chitosan (Karoichan et al., 2022), silk fibroin (Mehrabi et al., 2023), and alginate (Barros da Silva et al., 2020; Khalighi and Saadatmand, 2021). Additionally, decellularized adipose ECM has been investigated for adipocytic regeneration (Jeon et al., 2020; Lee et al., 2021; Li et al., 2018). Among crosslinking approaches (Campiglio et al., 2019), photocrosslinking has emerged as a promising approach to rapidly prepare mechanically stable hydrogels towards cell-friendly and cost-effective method. Photocrosslinking is a free radical chain-growth polymerization between the functional groups of polymer chains activated by light exposure (Moon et al., 2023). The polymeric material need to be properly functionalized via methacrylation throughout photo-sensible residues addition (Hu et al., 2019; Yang et al., 2023). A specific wavelength then excites an added photoinitiator (PI) causing the formation of chemical radicals, which propagate along polymeric backbone and establish covalent bonds among photo-sensible residues, building mechanically stable hydrogels.

Photocrosslinking processes for adipose TE have often involved gelatin methacrylate (GelMA) and UV irradiation (λ = 300–400 nm) (Chansoria et al., 2021; Grilli et al., 2022; Pepelanova et al., 2018; Zhang et al., 2023), even though several drawbacks were reported in literature, due to potential cellular DNA and tissues damages, genetic instabilities, and limited light penetration (Casey et al., 2017; Janmaleki et al., 2021; Lim et al., 2019; Tytgat et al., 2019; Young et al., 2020; M. Zhu et al., 2019a). To overcome these limitations, recent studies have been focused on using visible light instead of UV irradiation, mostly for neural (Kumar et al., 2021), bone (Goto et al., 2021; Moghanian et al., 2020; Paek et al., 2024) or cartilage applications (Lim et al., 2019, 2020; Paek et al., 2024).

Here, we developed biomimetic hydrogel scaffolds for AT engineering by mimicking the collagenous and glycosaminoglycan components of AT. GelMA and HA methacrylate (HAMA) were chosen as natural biomaterials to recapitulate adipose ECM; photocrosslinked hydrogels were fabricated via visible light exposure (λ = 405 nm), by using ruthenium (Ru) and sodium persulfate (SPS). Three different formulations of hybrid GelMA/HAMA hydrogels were prepared varying Ru/SPS concentrations, and physical and mechanical characterization was performed. Preadipocytes 3T3-L1 were encapsulated in GelMA/HAMA hydrogels to assess if developed constructs promoted cells proliferation. The adipogenic differentiation of 3T3-L1 in GelMA/HAMA hydrogels was further compared to GelMA samples, enlightening how HAMA addition in the polymeric network stimulated biochemical signals destined to preadipocytes and drove their differentiation.

2. Materials and methods

2.1. Materials

Materials were purchased from Sigma-Aldrich, unless differently specified: gelatin (from porcine skin, type A, gel strength ∼ 300 g Bloom), hyaluronic acid sodium salt from *Streptococcus equi* (HA, MW = 1.5–1.8 MDa), Dulbecco's Phosphate Buffered Saline (DPBS), methacrylic anhydride (MA), dialysis tubing (MWCO 12–14 kDa), 2-hydroxy-4'-(2-hydroxyethoxy)-2-methylpropiophenone (Irgacure 2959, I2959), Dulbecco's Modified Eagle's Medium (DMEM), resazurin sodium salt, calcein-AM, propidium iodide, sodium hydroxide, green phalloidin, DAPI. Chloro-(pentamethylcyclopentadienyl)-bis-(triphenylphosphine)-ruthenium(II) (Ruthenium visible light photoinitiator, Ru) and sodium persulfate (SPS) were purchased by Advanced Biomatrix. Silicon (PDMS, Elastosil RT 601 A-B) was purchased from WACKER. 3T3-L1 murine cells were obtained from the European Collection of Authenticated Cell Cultures (ECACC No 86052701).

2.2. Synthesis of gelatin methacrylate (GelMA) and hyaluronic acid methacrylate (HAMA)

GelMA was synthetized via methacrylation of gelatin (Van Den Bulcke et al., 2000). 10 g of gelatin powder were dissolved in 100 mL of DPBS at 50 °C. Methacrylation was performed by adding 8 mL of MA, and the reaction was carried out for 3 h at 50 °C under stirring. The obtained mixture was dialyzed, sterile filtered (∅ = 0.22 μm), frozen, and lyophilized. Methacrylation was verified by ^{1}H NMR spectroscopy (Bruker ARX 400 Instrument). The Degree of Functionalization (DoF) was determined as the percentage of methacrylated amino groups (Bilici et al., 2022) and calculated (Eq. (1)):

$$DoF_{GelMA}\ (\%) = \left[1 - \left(\frac{GelMA\ lysine\ groups}{Gel\ type\ A\ lysine\ groups}\right)\right] x100 \qquad \text{(Eq. 1)}$$

where: *GelMA lysine groups* and *Gel type A lysine groups* = integral area respectively of GelMA and gelatin lysine signals (2.9–3.1 ppm).

HAMA was synthetized via methacrylation of hyaluronic acid (Loebel et al., 2017). 2.5 g of HA powder were dissolved in 125 mL of distilled water at 4 °C. Subsequently, 9.66 mL of MA were added dropwise to HA solution and the pH was adjusted to 7.5–8.5 using 5 M NaOH during MA addition. The reaction was proceeded for 4 h, by maintaining the reaction mixture in the ice-water bath and monitoring the pH, dialyzed, frozen, lyophilized, and sterilized by autoclave. Methacrylation was verified by ^{1}H NMR spectroscopy. DoF was determined comparing the intensity of the signals of the vinyl groups of the methacrylates with the methacrylate methyl peak, as reported in Eq. (2) (Nedunchezian et al., 2022):

$$DoF_{HAMA}\ (\%) = \left[\frac{\frac{vinyl\ groups}{2}}{\frac{methacrylate\ methyl\ peak}{3}}\right] x100 \qquad \text{(Eq. 2)}$$

where: *vinyl groups* = intensity of the signal of the protons of the vinyl methacrylate peaks (5.8–6.2 ppm), *methacrylate methyl peak* = intensity of the signal of the three protons of the methyl methacrylate peak (∼ 1.9 ppm).

2.3. Hydrogel preparation

Hydrogels precursors were prepared by dissolving 10% w/V GelMA (GEL) or 10% w/V GelMA with 1% w/V HAMA (GEL _HA) in DPBS at 37 °C, and by adding different amounts of PI (0.05/0.5, 0.1/1, 0.2/2 mM/mM Ru/SPS, respectively). Hydrogels were prepared by pouring hydrogel precursors in PDMS molds (diameter ∅ = 8 mm, height h = 3 mm) and curing via visible light (λ = 405 nm) for 900 s (Portable Work

Light, Lotus Global co.). The obtained hydrogel library was composed of GelMA mixed with different amounts of PI (GEL_05, GEL_1, and GEL_2) and GelMA/HAMA blend hydrogels with different amounts of PI (GEL_HA_05, GEL_HA_1, and GEL_HA_2) (Table 1).

2.4. Physico-mechanical characterization

Crosslinked hydrogels were dehydrated via immersion in 50% v/V ethanol solution for 2 h, 100% ethanol for additional 2 h, and allowed to dry overnight. Anhydrous hydrogels (n = 5) were immersed in dH_2O (0.02% w/V NaN_3) and stored at 37 °C. At established time points (t = 1, 2, 3, 4, 24, 48, 72, 96 h and once a week up to 4 weeks), hydrogels were removed from the wells, gently dried on tissue paper to remove excess water, and weighted. The percentage weight variation (ΔW%) in time was calculated using Eq. (3) (Contessi Negrini et al., 2019b):

$$\Delta W(\%) = \frac{w_t - w_0}{w_0} x100 \quad \text{(Eq. 3)}$$

where: $\Delta W\%$ = percentage weight variation of each pure and hybrid hydrogels formulation, w_t = weight of swollen hydrogels at scheduled time points, w_0 = initial anhydrous weight.

The gel fraction, related to the percentage of hydrogel solid fraction retained by the samples at the swelling plateau (Contessi Negrini et al., 2019b), was measured at hydrogels swelling plateaus (t = 48 h for GEL, t = 24 h for GEL_HA). Anhydrous samples (n = 5) were weighted (w_a), incubated in dH_2O up to plateau, frozen (−20 °C), lyophilized, and weighted (w_l). The percentage gel fraction (G_f) was calculated using Eq. (4) (Contessi Negrini et al., 2019b; Tytgat et al., 2019):

$$G_f\% = \frac{w_a}{w_l} x100 \quad \text{(Eq. 4)}$$

where: w_a = anhydrous weight, w_l = lyophilized weight.

Mechanical compression tests were performed on swollen hydrogels (n = 3) by using a dynamic mechanical analyzer (DMA Q800, TA Instruments). Tests were carried out at 37 °C, after 0.001 N preload, in strain-controlled mode down to −30% strain at a strain rate of 2.5% min^{-1}, followed by an unloading phase up to −1% strain at 5% min^{-1} (Alkhouli et al., 2013; Contessi Negrini et al., 2019b; Tytgat et al., 2019). Mechanical parameters were calculated from stress/strain curves: elastic modulus E (0-2% strain range), stiffness K (5–15% strain range), maximum stress at 30% strain σ_{max}, residual strain ε_{res}, and hysteresis area H.

Rheological tests were performed by using a rotational rheometer (Anton Paar MCR 302 Modular Compact Rheometer, Anton Paar GmbH, Austria), equipped with parallel plate geometry (∅ = 25 mm, gap between plates = 95% of samples thickness (Contessi Negrini et al., 2019b)). Swollen hydrogels (∅ = 25 mm, h = 2 mm, n = 3) were preconditioned ($\dot{\gamma}$ = 0.01, f = 0.1 Hz for 60 s, and rest condition for 60 s). All tests were performed at 37 °C, and silicon oil was added to avoid samples drying. A strain sweep test ($\dot{\gamma}$ = 0.01–100%, F = 0.1 Hz) was performed to establish the Linear Viscoelastic Region (LVR). Then, frequency dependence of hydrogels rheological parameters was investigated with frequency sweep tests (f = 0.1–10 Hz; strain = 1% for GEL and 0.5% for GEL_HA, identified in LVR).

Table 1
List of GEL and GEL_HA hybrid hydrogels obtained by varying the concentration of Ru/SPS.

Hydrogels	GelMA (% w/V)	HAMA (% w/V)	Ru/SPS (mM/mM)
GEL_05	10	–	0.05/0.5
GEL_1	10	–	0.1/1
GEL_2	10	–	0.2/2
GEL_HA_05	10	1	0.05/0.5
GEL_HA_1	10	1	0.1/1
GEL_HA_2	10	1	0.2/2

2.5. In vitro biological tests: preadipocytes culture and differentiation

3T3-L1 preadipocytes were cultured in preadipocyte culture medium, composed by Dulbecco's Modified Eagle Medium (DMEM), 10% v/V fetal bovine serum (FBS), 1% v/V penicillin-streptomycin (P/S), 1 mM sodium pyruvate (PyR), 10 mM 4-(2-hydroxyethyl)-1-piperazine ethanesulfonic acid (HEPES), and 4 mM L-glutamine (Glut). 3T3-L1 preadipocytes (1×10^6 cell mL^{-1}) were encapsulated in hydrogel precursors (GEL_05, GEL_1, GEL_HA_05, GEL_HA_1) that were photo-crosslinked to obtain cell-laden hydrogel culture for 21 days.

Cell metabolism was evaluated by AlamarBlue assay at 1, 7, 14, 21 days after cells encapsulation; at each time point, 10% v/V AlamarBlue solution in DMEM was replaced to culture medium, samples were incubated for 4 h, 100 μL from each sample were transferred in triplicates into 96-multiwell, and fluorescence was read by using a spectrophotometer (Tecan, Genius Plus plate reader). Cell metabolic activity was measured in time as relative fluorescence unit (RFU, Eq. (5)) (Contessi Negrini et al., 2019b):

$$RFU_{encapsulated\ cells} = RFU_{cell-laden\ hydrogels} - RFU_{control\ hydrogels} \quad \text{(Eq. 5)}$$

Live/Dead staining was performed on cell-laden hydrogels after 3, 7, 14, 21 days (n = 3). Cell-laden hydrogels were washed with DPBS, immersed in staining solution (1 μM calcein-AM and 10 μM propidium iodide in DPBS), incubated for 40 min, washed with DPBS, and observed by fluorescent microscopy (Olympus BX51W1, live cells green, λ = 495 nm, and dead cell red, λ = 535 nm). Images (n = 3 per samples) were analyzed via ImageJ software.

Adipogenic differentiation was induced after 24 h of cultures in growth medium by culturing cells in differentiation medium (diff samples), containing growth medium supplemented with 0.5 mM of 3-isobutyl-1-methylxanthine (IBMX), 1 μg mL^{-1} of insulin, 1.0 μM of dexamethasone (DMX), 2.0 μM of rosiglitazone (ROX) (Yue et al., 2018). After 48 h, differentiation medium was changed with maintenance medium, composed by growth medium with 1 μg mL^{-1} of insulin, changed every two days. Metabolic activity of cells during adipogenic differentiation was investigated via AlamarBlue assay (n = 5, as previously described). Cells embedded in the same hydrogel formulations were cultured in growth medium (ndiff samples) up to 21 days and used as control. Adipogenic differentiation was quantitatively investigated via Oil Red O (ORO) and qualitatively by Nile Red staining, after 21 days of culture. ORO staining solution was prepared by dissolving 300 mg ORO powder in 100 mL 2-propanol, followed by dilution in distilled water (2:3 = dH_2O:ORO stock solution) and sterile filtration. Differentiated (n = 3) and undifferentiated (n = 3) samples were fixed in 4% paraformaldehyde for 1 h at RT, washed twice with DPBS and immersed in ORO staining solution for 1 h at 37 °C avoiding light exposure. Then, hydrogels were washed five times with sterile dH_2O, and visualized by optical microscope (Leica, Wild M8). Lipid accumulation was quantified by immersing hydrogels in 2-propanol overnight to extract the ORO staining solution, manually broken with a pestle and the obtained eluates were transferred in a 48-multiwell. The eluates absorbance was read at λ = 510 nm (Giudetti et al., 2020; Kraus et al., 2016) and converted into ORO concentration (i.e., corresponding to lipidic droplets accumulation) via a calibration curve. Nile Red staining was performed to qualitatively checked 3T3-L1 intracellular lipid accumulation. Briefly, differentiated (n = 3) and undifferentiated (n = 3) hydrogels were fixed with 4% paraformaldehyde, immersed in 0.25% v/V Triton X, and stained by adding staining solution. Staining solution was prepared by supplemented in sterile DPBS 1000 μg mL^{-1} Nile Red and 7 μg mL^{-1} green phalloidin.

2.6. Statistical analysis

All data are expressed as mean ± standard deviation. Shapiro-Wilk normality test was performed to check normal distribution. One-way ANOVA tests multiple comparison, and unpaired *t*-test were performed

with GraphPad Prism software; $p < 0.05$ was set as statistically significant threshold.

3. Results

3.1. Synthesis of GelMA and HAMA

Representative ^{1}H NMR spectra of pristine gelatin, gelatin methacrylate (GelMA), HA, and HA methacrylate (HAMA) are reported in Fig. 1. ^{1}H NMR spectra confirmed the successful methacrylation of both polymers. The gelatin spectra (Fig. 1A) show the appearance of peaks at around 5.25–5.75 ppm, which were attributed to acrylic protons of methacryloyl grafts, which could be distinguished in acrylic methacrylate (a + b) and methacrylamide (c) groups, obtained by functionalization of ammine (lysine) and hydroxyl (hydroxylysine) groups, respectively. The lysine methylene peak at 2.9–3.1 ppm was the highest in gelatin spectrum, while decreased in GelMA signal, due to the chemical functionalization. Aromatic proton signals remained constant in both upper and lower spectra at 7.1–7.4 ppm. The DoF for GelMA was 56%. In HAMA spectrum, new peaks appeared (Fig. 1B), referred to the functionalization of hydroxyl groups (d) of N-acetyl glucosamine monosaccharide unit, and to the methacrylate groups formation (a: 1.9 ppm, b + c: 5.6–6.3 ppm), due to the chemical reaction. The DoF for HAMA was 27%.

3.2. In vitro stability tests

Both GEL and GEL_HA hydrogel formulations prepared by varying Ru and SPS concentrations successfully formed after exposure to visible light. Reaction schemes are reported in Fig. 2A, respectively for GEL **(i)** and GEL_HA **(ii)** hydrogels. GEL hydrogels exhibited an increase in weight due to water absorption up to the swelling plateau (48 h for all GEL samples, Fig. 2B (i), left); after that, weight variation was stable up to 4 weeks of immersion in water ($p > 0.05$). GEL_05 showed the highest weight variation at plateau (Fig. 2B (ii), left; $p < 0.01$ vs GEL_1, $p < 0.0001$ vs GEL_2), followed by GEL_1, and GEL_2 that showed the lowest increase in weight ($p < 0.0001$ vs GEL_05, $p < 0.001$ vs GEL_1).

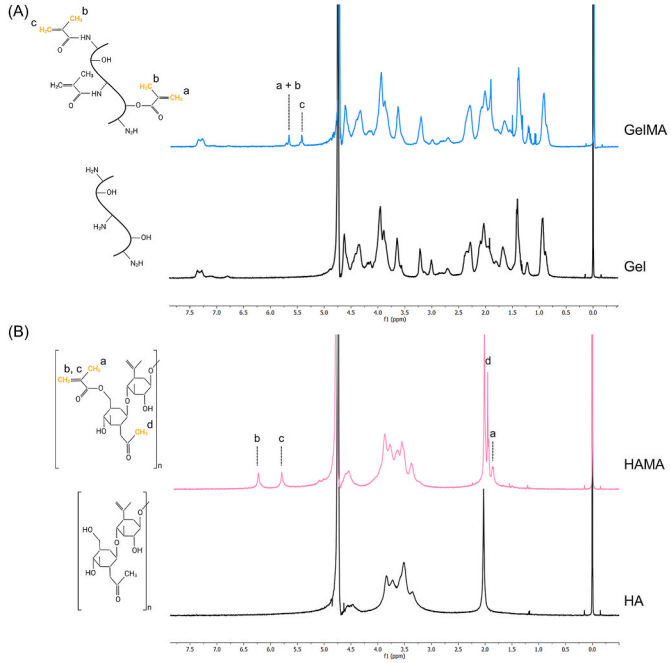

Fig. 1. Representative chemical structures and ^{1}H NMR spectra of (A) gelatin methacrylate (GelMA, top) and gelatin (Gel, bottom), and (B) hyaluronic acid methacrylate (HAMA, top) and hyaluronic acid (HA, bottom).

Moreover, GEL_05 hydrogels were characterized by a lower gel fraction ($p < 0.01$ vs GEL_1, $p < 0.001$ vs GEL_2) (Fig. SM1A) than other GEL hydrogels. The amount of PI influenced the swelling properties of the hydrogels, as an increase in PI led to lower swelling degree.

A similar trend was observed for GEL_HA hydrogels weight variation (Fig. 2B (i), right). After a sharp increase in weight in the first 24 h, all samples reached constant weight variation values up to 4 weeks ($p > 0.05$); as for GEL hydrogels, lower amount of PI led to higher weight variation at plateau. The highest weight variation at plateau was observed for GEL_HA_05 (Fig. 2B (ii), right; $p < 0.01$ vs GEL_HA_1, $p < 0.001$ vs GEL_HA_2). By considering GEL_HA_2 hydrogels, their water uptake resulted comparable to GEL_HA_1, since their tighter polymeric network allowed to potentially entrap a higher amount of HAMA which balanced the water uptake. Gel fraction resulted lower for GEL_HA_05 ($p < 0.05$ vs GEL_HA_1, $p < 0.01$ vs GEL_HA_2) than other GEL_HA hydrogels (Fig. SM1B). Moreover, no statistical differences in gel fraction values were reported for GEL_HA_1 and GEL_HA_2, confirming the comparable results obtained from weight variation tests.

By comparing weight variations kinetics between GEL hydrogels and GEL_HA hybrid hydrogels, GEL_HA exhibited a higher degree of swelling and consequently entrapped a higher amount of water than GEL samples (Fig. SM2A; $p < 0.01$ GEL_05 vs GEL_HA_05, $p < 0.01$ GEL_1 vs GEL_HA_1, $p < 0.001$ GEL_2 vs GEL_HA_2), that can be associated to the highly hydrophilic nature of hyaluronic acid (Karousou et al., 2014). A comparison between gel fraction of GEL and hybrid hydrogels was also carried out, and significative differences were not found (Fig. SM2B).

3.3. Mechanical compression test

Representative mechanical compressive stress-strain (σ-ε) curves of swollen GEL hydrogels are shown in Fig. 2C (i) (**left**). GEL hydrogels exhibited a hysteresis cycle typical of viscoelastic materials (Contessi Negrini et al., 2019b). An increase in hydrogels stiffness was observed by increasing the amount of PI (Fig. 2C (ii), **left**). GEL_2 showed the highest stiffness ($K = 10.48 \pm 0.08$ kPa), followed by GEL_1, and GEL_05, attributed to the higher density of crosslinking that can be formed by increasing the amount of PI. The obtained mechanical properties for GEL_1 samples ($K = 7.07 \pm 1.13$ kPa) were comparable to the ones (12.8 kPa) of GEL hydrogels photocrosslinked with the same amount of PI (Ru/SPS = 0.1/1 mM/mM), while GEL_2 hydrogels exhibited lower values of stiffness ($K = 10.48 \pm 0.08$ kPa) compared to similar formulations reported in literature (31.6 kPa) (Lim et al., 2019). This difference might be attributable to the different instrument equipped for photocrosslinking. Other mechanical parameters calculated for GEL samples (elastic modulus, maximum stress, residual deformation, and hysteresis area) are reported in **SM3.A**.

Representative σ-ε curves of GEL_HA hydrogel formulations are reported in Fig. 2C (i) (**right**), exhibiting the typical viscoelastic hysteresis cycle. Obtained stiffness is reported in Fig. 2C (ii), **right**, while other calculated mechanical parameters for GEL_HA hydrogels in **SM3.B** (elastic modulus, maximum stress, residual deformation, and hysteresis area). The lowest stiffness was exhibited by GEL_HA_05 formulation ($K = 15.84 \pm 1.18$ kPa, $p < 0.05$ vs GEL_HA_1 and GEL_HA_2), obtained with the lowest amount of Ru/SPS. Increasing the PI concentration, no significative differences were detected comparing GEL_HA_1 and GEL_HA_2 ($p > 0.05$), confirming the results obtained in weight variation tests.

GEL_HA hydrogels were characterized by higher stiffness compared to GEL samples obtained with the same amount of Ru/SPS (Fig. SM2C (i)-(ii)). This finding agreed with what Camci-Unal et al. showed in their work (Camci-Unal et al., 2013), where combination at different concentrations of HAMA (0, 1, 2% w/V) and GelMA (3, 5, 10% w/V) led to a significant increase in stiffness due to the presence of HAMA into polymeric network, after UV exposure.

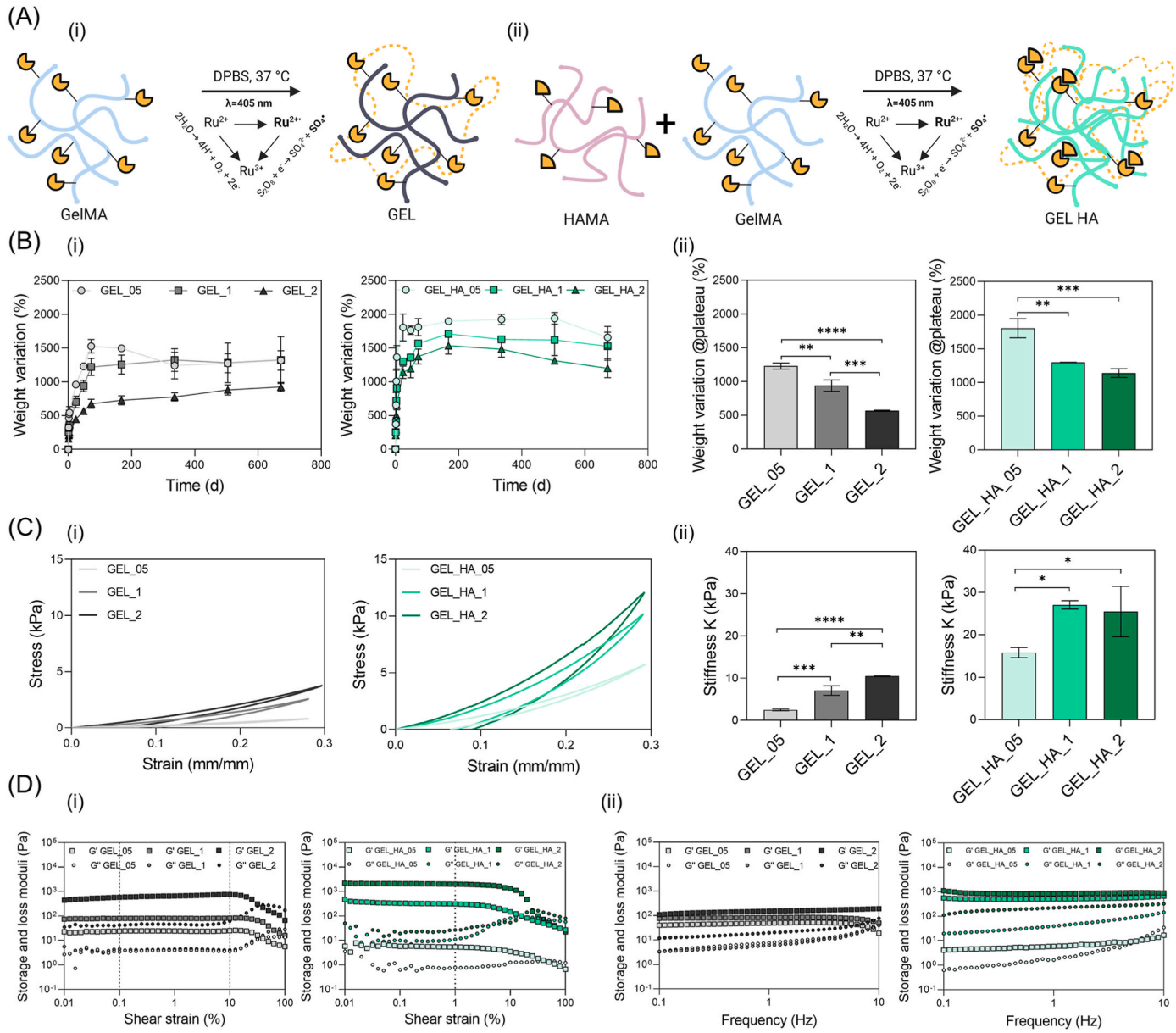

Fig. 2. Gelatin (GEL) and gelatin/hyaluronic acid (GEL_HA) hydrogels, n = 3 per formulation; data are expressed as mean ± standard deviation. (A) Schematic of the preparation of GEL (i) and GEL_HA (ii) hydrogels via Ru/SPS mediated visible light photocrosslinking. (B) Weight variation (i) and swelling at plateau (ii) of GEL and GEL_HA obtained with different amount of PI (0.5, 1, and 2 mM). (C) Representative stress-strain (σ-ε) curves of swollen hydrogels (i) and stiffness (ii). (D) Rheological properties of GEL and GEL_HA via strain sweep (i) and frequency sweep tests (ii). (*) $p < 0.05$, (**) $p < 0.01$, (***) $p < 0.001$, (****) $p < 0.0001$.

3.4. Rheological tests

All crosslinked hydrogels showed predominant storage modulus G′ over the loss modulus G″ during the strain sweep ramps (Fig. 2D (i)). The frequency response of the hydrogels varied depending on the amount of PI. GEL_2 samples showed a G′ higher than G″ in the considered frequency range (0.1–10 Hz), while GEL_1 and GEL_05 exhibited a decrease in G′ from 5 to 10 Hz (Fig. 2D (ii)). Contrarily, storage modulus in hybrid GEL_HA samples remained constant (GEL_HA_2) or increased (GEL_HA_05, GEL_HA_1) in the defined frequency range, exhibiting a behavior typical of crosslinked hydrogels with a solid-like response (Contessi Negrini et al., 2019b). Lastly, by calculating tanδ for fabricated hydrogels, all obtained values resulted much lower than 1, enlightening how samples behaved as elastic solid with a well-developed crosslinked network (Hou et al., 2021). For strains higher than the LVR limit (0.1–10% and 0.01–1%, respectively for GEL and GEL_HA), G' decreases due to the rupture of the hydrogel microstructure (Camci-Unal et al., 2013). All hydrogels were characterized by a shear-thinning behavior for all GEL and GEL_HA formulations, as evidenced by decreasing complex viscosity with increasing shear rate (**SM4**).

In general, different values of G′ were obtained by adding HA to GEL and by varying Ru/SPS concentration. GEL_HA hydrogels showed higher G' compared to GEL hydrogels obtained with the same amount of PI, except for GEL_05 vs GEL_HA_05 samples, where the higher water uptake might balance the formation of a denser polymeric network due to the presence of HAMA.

3.5. In vitro preadipocytes culture

For biological *in vitro* tests, GEL_05, GEL_1, GEL_HA_05 and GEL_HA_1 samples were tested, since GEL_HA_2 resulted comparable with GEL_HA_1 in terms of weight variation, gel fraction and mechanical

properties (GEL_2 was at the same time excluded). To verify the cytocompatibility of the employed photocrosslinking process, Live/Dead staining was performed after 72 h of cells encapsulation (i.e., swelling plateau for GEL and GEL_HA hydrogels) and revealed how most of the cells resulted viable (Fig. SM5). The metabolic activity of preadipocytes encapsulated in GEL and GEL_HA hydrogels, expressed as RFUs measured by Alamar Blue assay, is shown in Fig. 3A. The metabolic activity increased until 21 days of culture ($p < 0.05$) in GEL_05, while resulted stable ($p > 0.05$) during the first 14 days of culture in GEL_1, evidencing an increase only from day 14 to day 21 ($p < 0.05$). Live/Dead staining qualitatively confirmed this different proliferation rate, evidencing the presence of multiple red spots in GEL_1 after 7 days of culture (**SM5**).

In GEL_HA samples, the fluorescence signal was stable during the first 7 days of culture ($p > 0.05$); after that, the metabolic activity increased for all the considered time points ($p < 0.05$), both in GEL_HA_05 and GEL_HA_1, as observable in Live/Dead staining, where viable cells homogeneously colonized the microenvironment starting by 7 days of culture (**SM6**). Moreover, fluorescence signals resulted higher for GEL_HA_05 (i.e., the softest) than GEL_HA_1 (i.e., the stiffest) during all the considered time points ($p < 0.05$ at day 1, $p < 0.01$ at day 7, $p < 0.001$ at day 14, $p < 0.01$ at day 21).

By comparing metabolic activity of encapsulated preadipocytes in GEL and hybrid hydrogels, GEL_HA hydrogels exhibited higher RFUs values than the GEL formulation crosslinked with the same amount of Ru/SPS at each considered time point. These differences in fluorescence signals enlightened how HAMA presence in the polymeric network promoted preadipocytes proliferation. Live/Dead staining qualitatively confirmed the presence of viable, adherent, and elongated cells encapsulated in GEL and GEL_HA hydrogels after 21 days of culture (Fig. 3B).

3.6. *In vitro preadipocytes differentiation into mature adipocytes*

Once assessed the capability of GEL and GEL_HA hydrogels in supporting preadipocytes growth, hydrogels were investigated to evaluate their capability in promoting an active metabolic functionality of encapsulated cells. For this purpose, preadipocytes-laden samples were cultured in differentiation culture medium for 48 h, then replaced with maintenance medium (diff samples). Lipid accumulation in diff samples was compared with preadipocytes cultured in standard conditions (ndiff samples), cultured up to 21 days in growth medium. After 21 days of culture, round-shaped intracellular lipidic droplets were evidenced in diff_GEL and diff_GEL_HA samples compared to ndiff hydrogels via Nile Red staining (Fig. 4A). A higher amount of lipidic droplets was qualitatively detectable in diff_GEL_HA_05 hydrogels compared to diff_GEL_05, diff_GEL_1, and diff_GEL_HA_1. Accumulation of lipidic droplets was not noticed in ndiff samples for both correspondent GEL and GEL_HA hydrogels (Fig. 4A).

The successful adipogenic differentiation of preadipocytes encapsulated in diff_GEL and diff_GEL_HA hydrogels was proved by ORO staining quantification (Fig. 4B). Consistently with Nile Red staining, a significantly higher ORO concentration was measured in the isopropanol elution of ORO staining of all diff samples hydrogels than ndiff hydrogels ($p < 0.05$) (**SM6**). Differentiation degree resulted higher in hydrogels with lower amount of Ru/SPS, as diff_GEL_05 and diff_GEL_HA_05 showed a higher ORO quantification than diff_GEL_1 ($p < 0.0001$ vs diff_GEL_05) and diff_GEL_HA_1 ($p < 0.0001$ vs diff_GEL_HA_05), respectively (Fig. 4B). This finding agreed with proliferation rate of encapsulated preadipocytes since a denser polymeric network due to a higher Ru/SPS concentration limited preadipocytes metabolic activity and differentiation, consequently. Moreover, ORO quantification allowed to enlighten how HAMA addition promoted a higher differentiation degree than GEL samples since preadipocytes better differentiated in hybrid diff_GEL_HA hydrogels than diff_GEL samples ($p < 0.05$).

4. Discussion

We developed 3D biomaterial-based *in vitro* models of AT by mimicking two relevant adipocytic ECM components: gelatin, a collagen derivative containing cell-adhesion motifs (RGD), and HA, which regulates water uptake in tissue ECM (Freedman and Mooney, 2019). Visible light approaches recently gained attention to obtain crosslinked hydrogels, e.g., gelatin (Khanmohammadi et al., 2019), decellularized ECM (Kim et al., 2021), silk fibroin (Cui et al., 2020). In this work, we fabricated GEL and GEL_HA formulations by varying Ru/SPS concentrations, to select which one (or ones) better promoted lipid accumulation, supporting preadipocytes differentiation towards adipocytes in AT-like microenvironment. We functionalized gelatin and HA and achieved DoFs comparable to other GelMA (56%) and HAMA (27%) reported in literature (Camci-Unal et al., 2013; Hachet et al., 2012; Lim et al., 2019; Loebel et al., 2017). Upon exposure to visible light, excited Ru cleaves SPS molecules, forming radical sulphates, able to promote crosslinks (Lim et al., 2019). All the formulations we tested resulted

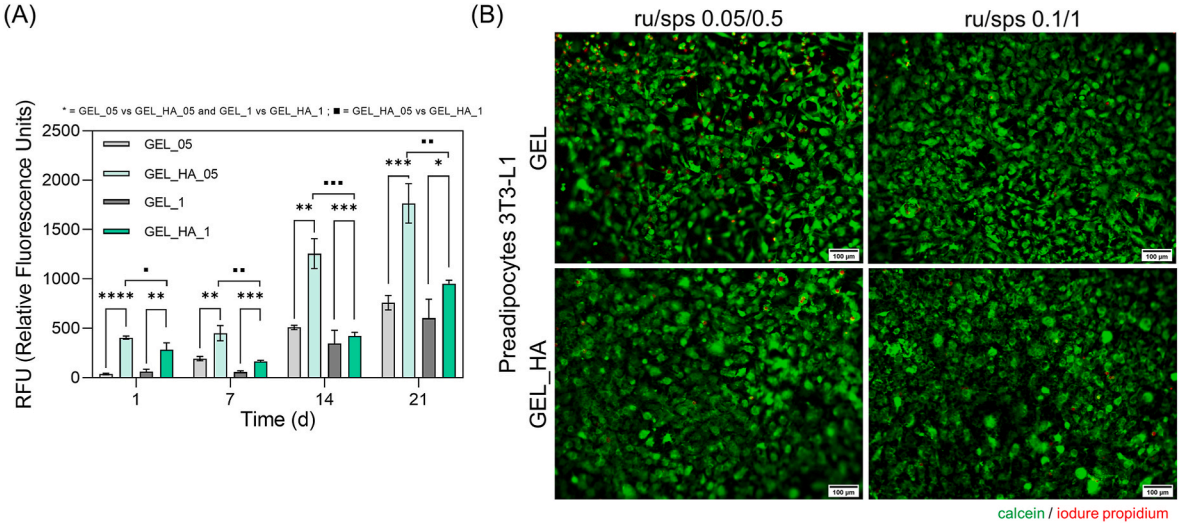

Fig. 3. 3T3-L1 preadipocytes proliferation in hydrogels. (A) AlamarBlue assay results after 1, 7, 14, 21 days of cell culture (n = 5 per formulation). (B) Live/Dead staining (scale bar: 100 μm) after 21 days of culture (n = 3 per formulation). GEL_05 vs GEL_HA_05, GEL_1 vs GEL_HA_1: (*) $p < 0.05$, (**) $p < 0.01$, (***) $p < 0.001$, (****) $p < 0.0001$. GEL_HA_05 vs GEL_HA_1: (■) $p < 0.05$, (■■) $p < 0.01$, (■■■) $p < 0.001$.

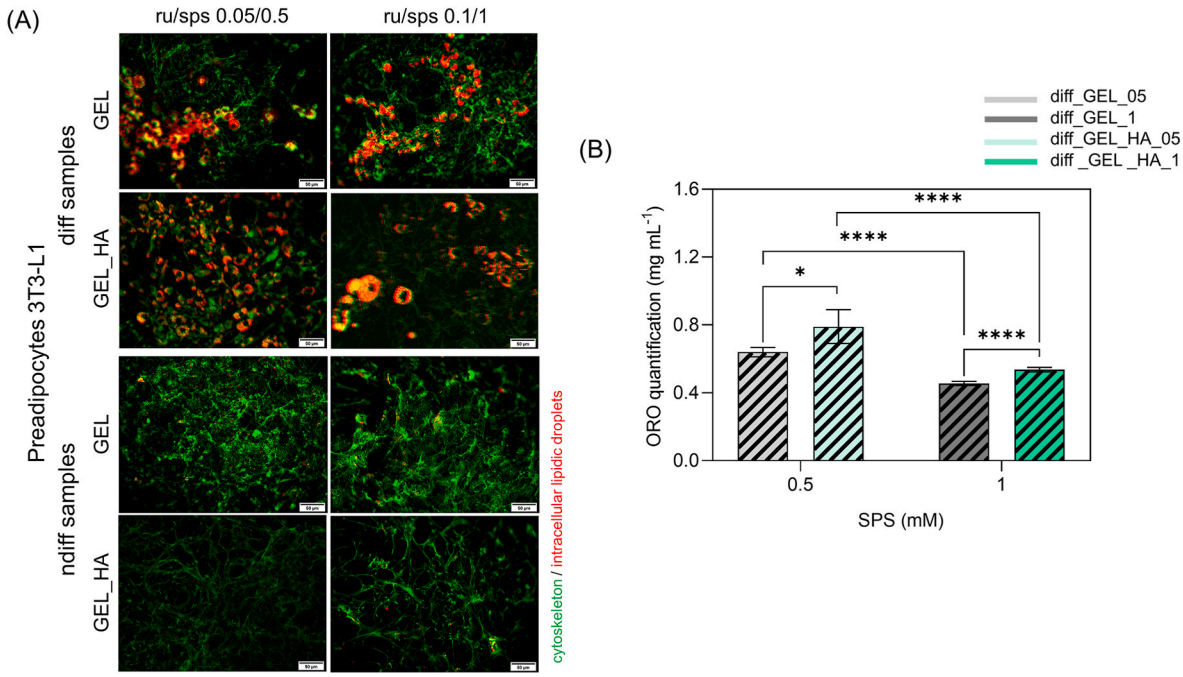

Fig. 4. 3T3-L1 preadipocytes differentiation in hydrogels. (A) Nile Red staining (scale bar: 50 μm) after 21 days of cell culture (n = 3 per formulation). (B) ORO quantification via absorbance for diff samples (n = 3 per formulation). (*) $p < 0.05$, (**) $p < 0.01$, (***) $p < 0.001$, (****) $p < 0.0001$.

stable in water at 37 °C with swelling trends and mechanical/rheological properties comparable to what observed in other literature works (Kim et al., 2021; Lim et al., 2019). Lim et al. fabricated GelMA hydrogels by varying Ru/SPS and observed how samples photocrosslinked with the lowest PI possessed the highest swelling ability and lowest mechanical properties. Same observations were expressed by Kim et al., who developed decellularized ECM hydrogels by varying Ru/SPS concentration. Furthermore, the *in vitro* biological tests performed on GEL_05, GEL_1, GEL_HA_05, and GEL_HA_1 showed how preadipocytes proliferated and differentiated better in softer hydrogels with higher water uptake capability (GEL_HA_05). As comparison, we also prepared HAMA hydrogels (**SM7**), by varying Ru/SPS concentrations (HA_05, HA_1, HA_2). Among the prepared formulations, HA_1 and HA_2 resulted weaker in terms of stability and degraded after 1 week and 96 h, respectively; these results agreed with the literature findings that SPS accelerated the degradation of the HA molecules (Hong et al., 2019). For this reason, we did not consider HA_1 and HA_2 formulations for further *in vitro* biological studies. Contrarily, HA_05 hydrogels were stable up to 2 weeks, and when 3T3-L1 preadipocytes were embedded in HA_05 hydrogels, cells resulted viable after 7 days of culture (**SM7**). However, rapid degradation of HA_05 hydrogels (2 weeks) prevented from longer *in vitro* cultures (e.g., more than 2 weeks) and lipid accumulation investigation.

However, the inclusion of HAMA in GelMA polymeric network (GEL_HA formulations) ensured a greater water uptake and higher mechanical/rheological properties compared to GEL samples, accordingly with literature. Indeed, the addition of natural materials (e.g., alginate, gellan gum methacrylate, chondroitin sulfate methacrylate, silk fibroin, dextran methacrylate, HA) in GelMA hydrogels improved their mechanical properties (Camci-Unal et al., 2013; Sakr et al., 2022), possibly influencing cell fate, as observed for our formulations and in literature (Chansoria et al., 2021; Pepelanova et al., 2018). Pepelanova et al. investigated mesenchymal stem cells (MSCs) proliferation in GelMA hydrogels crosslinked with different UV intensities (1.2 vs 2.4 J cm^{-2}), observing an increased cell viability after polymerization with lower intensity, due to a lower crosslinking, causing softer hydrogels. Additionally, Chansoria et al. obtained hydrogels by varying GelMA concentration and light exposure time. The material stiffness (0.25–17.00 kPa) influenced cells response: in high stiffness hydrogels, preadipocytes could not remodel the surrounding matrix and exhibited a less elongated morphology, whereas at very low stiffness, cellular spheroids were formed. This stiffness-dependent cell behavior agreed with preadipocytes behavior cultured in our GEL and GEL_HA hydrogels. Adipogenic differentiation was preliminarily assessed in our GEL and GEL_HA hydrogels: the presence of HAMA enhanced lipid accumulation in GEL_HA samples and offered a more biomimetic adipocytic ECM compared to GEL formulations. To the best of our knowledge, GelMA/HAMA hydrogels were not developed in literature for mimicking AT; some papers investigated this hybrid formulation for intervertebral disc repair (Chen et al., 2019), cartilage engineering (Nedunchezian et al., 2022), or bone matrix formation (Wenz et al., 2018), where the requirements (e.g., stiffness) are different and peculiar to promote the tissue-specific cells viability. Moreover, stiffness of our GEL and GEL_HA formulations fit the values reported in literature for human breast adipose ECM (0.50–25.00 kPa) (Contessi Negrini et al., 2019b; Zhang et al., 2023), and G' of GEL and GEL_HA hydrogels (i.e., ranging from 4 to 1100 Pa) were comprised in the values reported in literature for scaffolds for liver, relaxed muscle, breast, and gland tissues (Velasco-Rodriguez et al., 2021). Hence, we showed that varying the Ru/SPS ratio, we are able to obtain GEL and GEL_HA hydrogels that can appropriately mimic the stiffness of different soft tissues, so that they can be considered a sort of library to choose the composition that better suits the main mechanical requirement for the *in vitro* mimicking or for the *in vivo* regeneration of a specific soft tissue.

Blending HAMA in GelMA network showed also to biochemically stimulate encapsulated preadipocytes influencing lipid accumulation. HA proved adipogenic potential and resulted the optimal choice for *in vivo* transplantation of preadipocytes or adipocyte stem cells (ASCs) (Y. Zhu et al., 2019a). Moreover, an increased lipid accumulation, that could relate to more efficient adipogenic differentiation of preadipocytes, was observed when cells were encapsulated in crosslinked HA scaffolds towards carboxyl groups amidation (Y. Zhu et al., 2019b); interestingly, degree of lipid accumulation resulted correlated with the degree of crosslinking of the HA scaffolds. Lipid accumulation is mainly influenced by the stiffness of the cell-laden matrix as well as by the cell density. As an example, Yue et al. showed that UV crosslinked GelMA

hydrogels promoted adipogenic differentiation in soft hydrogels (0.25–3.00 kPa), and in particular when a higher cell density was studied (from 1×10^6 to 1×10^7 cells mL^{-1}), a higher lipid droplet deposition occurred (Yue et al., 2018). However, in our formulations, the presence of HAMA played a relevant role in preadipocyte differentiation even at low cell density (1×10^6 cells mL^{-1}), possibly due to the biochemical microenvironment more similar to the native one (15.84–27.05 kPa). Understanding how scaffold chemical composition and stiffness influences preadipocytes metabolism could represent the first step in studying the complex plethora of cell-ECM interactions in adipocytic ECM and the possible origin of mutations which trigger tumors or AT pathologies. Among the formulations here investigated, GEL_HA hydrogels resulted suitable candidates for mimicking native AT, in terms of stiffness and lipid accumulation.

The results of the current study enlighten that AT scaffold features affect adipocytes differentiation in a stiffness-dependent manner, and pointed out that fabricating hybrid hydrogels with tunable properties will allow a better adipocytic ECM mimicry. Our hydrogels allow to obtain versatile structures to investigate cells behavior in a native-like adipose ECM, but the possibility to tune their properties increases the application of our formulations in pathological-like ECM. Future perspectives might be focused on the culture of pathological cell lines which could resemble inflammatory conditions of breast AT in a breast tumor-like ECM. The advantage related to the possibility of tailoring hydrogel features allows to produce hydrogels with different degrees of stiffness, opening the chance to study aggressiveness and invasiveness of breast cancer cells in surrounding ECM.

5. Conclusions

We prepared hydrogels to mimic the physico-mechanical properties and ECM components of AT by combining gelatin and HA via visible light photocrosslinking. We modulated the properties of the prepared hydrogels by changing the concentration of PI to obtain hydrogels stable for more than 4 weeks at 37 °C and with mechanical properties suitable to mimic healthy breast AT (GEL) and stiffened breast cancer AT. The hydrogels successfully supported preadipocyte adhesion, proliferation, and adipogenic differentiation, resulting in a promising 3D model for future encapsulation of further relevant cell populations and to recreate a more complex breast AT model.

CRediT authorship contribution statement

Matteo Pitton: Writing – original draft, Validation, Methodology, Investigation, Formal analysis, Data curation, Conceptualization. **Christian Urzì:** Validation, Methodology, Investigation, Formal analysis, Data curation, Conceptualization. **Silvia Farè:** Writing – review & editing, Writing – original draft, Supervision, Project administration, Conceptualization. **Nicola Contessi Negrini:** Writing – review & editing, Writing – original draft, Supervision, Project administration, Conceptualization.

Declaration of competing interest

The authors declare that they have no known competing financial interests or personal relationships that could have appeared to influence the work reported in this paper.

Data availability

The data that has been used is confidential.

Appendix A. Supplementary data

Supplementary data to this article can be found online at https://doi.org/10.1016/j.jmbbm.2024.106675.

References

Alkhouli, N., Mansfield, J., Green, E., Bell, J., Knight, B., Liversedge, N., Tham, J.C., Welbourn, R., Shore, A.C., Kos, K., Winlove, C.P., 2013. The mechanical properties of human adipose tissues and their relationships to the structure and composition of the extracellular matrix. Am. J. Physiol. Endocrinol. Metab. 305, E1427–E1435. https://doi.org/10.1152/ajpendo.00111.2013.

Avtanski, D., Hadzi-Petrushev, N., Josifovska, S., Mladenov, M., Reddy, V., 2023. Emerging technologies in adipose tissue research. Adipocyte 12, 2248673. https://doi.org/10.1080/21623945.2023.2248673.

Bahcecioglu, G., Basara, G., Ellis, B.W., Ren, X., Zorlutuna, P., 2020. Breast cancer models: engineering the tumor microenvironment. Acta Biomater. 106, 1–21. https://doi.org/10.1016/j.actbio.2020.02.006.

Barros da Silva, P., Coelho, M., Bidarra, S.J., Neves, S.C., Barrias, C.C., 2020. Reshaping in vitro models of breast tissue: integration of stromal and parenchymal compartments in 3D printed hydrogels. Front. Bioeng. Biotechnol. 8, 494. https://doi.org/10.3389/fbioe.2020.00494.

Bilici, Ç., Tatar, A.G., Şentürk, E., Dikyol, C., Koç, B., 2022. Bisulfite-initiated crosslinking of gelatin methacryloyl hydrogels for embedded 3D bioprinting. Biofabrication 14, 025011. https://doi.org/10.1088/1758-5090/ac4dd9.

Camci-Unal, G., Cuttica, D., Annabi, N., Demarchi, D., Khademhosseini, A., 2013. Synthesis and characterization of hybrid hyaluronic acid-gelatin hydrogels. Biomacromolecules 14, 1085–1092. https://doi.org/10.1021/bm3019856.

Campiglio, C.E., Contessi Negrini, N., Farè, S., Draghi, L., 2019. Cross-Linking strategies for electrospun gelatin scaffolds. Materials 12, 2476. https://doi.org/10.3390/ma12152476.

Casey, J., Yue, X., Nguyen, T.D., Acun, A., Zellmer, V.R., Zhang, S., Zorlutuna, P., 2017. 3D hydrogel-based microwell arrays as a tumor microenvironment model to study breast cancer growth. Biomed. Mater. 12, 025009 https://doi.org/10.1088/1748-605X/aa5d5c.

Chansoria, P., Asif, S., Polkoff, K., Chung, J., Piedrahita, J.A., Shirwaiker, R.A., 2021. Characterizing the effects of synergistic thermal and photo-cross-linking during biofabrication on the structural and functional properties of gelatin methacryloyl (GelMA) hydrogels. ACS Biomater. Sci. Eng. 7, 5175–5188. https://doi.org/10.1021/acsbiomaterials.1c00635.

Chen, P., Ning, L., Qiu, P., Mo, J., Mei, S., Xia, C., Zhang, J., Lin, X., Fan, S., 2019. Photo-crosslinked gelatin-hyaluronic acid methacrylate hydrogel-committed nucleus pulposus-like differentiation of adipose stromal cells for intervertebral disc repair. J. Tissue Eng. Regen. Med. 13, 682–693. https://doi.org/10.1002/term.2841.

Chuang, C.-H., Lin, R.-Z., Melero-Martin, J.M., Chen, Y.-C., 2018. Comparison of covalently and physically cross-linked collagen hydrogels on mediating vascular network formation for engineering adipose tissue. Artif. Cells, Nanomed. Biotechnol. 46, 434–447. https://doi.org/10.1080/21691401.2018.1499660.

Contessi Negrini, N., Bonnetier, M., Giatsidis, G., Orgill, D.P., Farè, S., Marelli, B., 2019a. Tissue-mimicking gelatin scaffolds by alginate sacrificial templates for adipose tissue engineering. Acta Biomater. 87, 61–75. https://doi.org/10.1016/j.actbio.2019.01.018.

Contessi Negrini, N., Celikkin, N., Tarsini, P., Farè, S., Święszkowski, W., 2020. Three-dimensional printing of chemically crosslinked gelatin hydrogels for adipose tissue engineering. Biofabrication 12, 025001. https://doi.org/10.1088/1758-5090/ab56f9.

Contessi Negrini, N., Tarsini, P., Tanzi, M.C., Farè, S., 2019b. Chemically crosslinked gelatin hydrogels as scaffolding materials for adipose tissue engineering. J. Appl. Polym. Sci. 136, 47104 https://doi.org/10.1002/app.47104.

Cui, X., Soliman, B.G., Alcala-Orozco, C.R., Li, J., Vis, M.A.M., Santos, M., Wise, S.G., Levato, R., Malda, J., Woodfield, T.B.F., Rnjak-Kovacina, J., Lim, K.S., 2020. Rapid photocrosslinking of silk hydrogels with high cell density and enhanced shape fidelity. Adv. Healthcare Mater. 9, 1901667 https://doi.org/10.1002/adhm.201901667.

Di Caprio, N., Bellas, E., 2020. Collagen stiffness and architecture regulate fibrotic gene expression in engineered adipose tissue. Adv. Biosyst. 4, 1900286 https://doi.org/10.1002/adbi.201900286.

Di Stefano, A.B., Massihnia, D., Grisafi, F., Castiglia, M., Toia, F., Montesano, L., Russo, A., Moschella, F., Cordova, A., 2019. Adipose tissue, angiogenesis and angio-MIR under physiological and pathological conditions. Eur. J. Cell Biol. 98, 53–64. https://doi.org/10.1016/j.ejcb.2018.11.005.

Domingues, M., Leite Pereira, C., Sarmento, B., Castro, F., 2023. Mimicking 3D breast tumor-stromal interactions to screen novel cancer therapeutics. Eur. J. Pharmaceut. Sci. 190, 106560 https://doi.org/10.1016/j.ejps.2023.106560.

Flont, M., Dybko, A., Jastrzębska, E., 2023. A layered cancer-on-a-chip system for anticancer drug screening and disease modeling. Analyst 148, 5486–5495. https://doi.org/10.1039/D3AN00959A.

Freedman, B.R., Mooney, D.J., 2019. Biomaterials to mimic and heal connective tissues. Adv. Mater. 31, 1806695 https://doi.org/10.1002/adma.201806695.

Ghaffari-bohlouli, P., Simińska-Stanny, J., Jafari, H., Mirzaei, M., Nie, L., Delporte, C., Shavandi, A., 2023. Printable hyaluronic acid hydrogel functionalized with yeast-derived peptide for skin wound healing. Int. J. Biol. Macromol. 232, 123348 https://doi.org/10.1016/j.ijbiomac.2023.123348.

Giudetti, A.M., Guerra, F., Longo, S., Beli, R., Romano, R., Manganelli, F., Nolano, M., Mangini, V., Santoro, L., Bucci, C., 2020. An altered lipid metabolism characterizes Charcot-Marie-Tooth type 2B peripheral neuropathy. Biochim. Biophys. Acta BBA - Mol. Cell Biol. Lipids 1865, 158805. https://doi.org/10.1016/j.bbalip.2020.158805.

Goto, R., Nishida, E., Kobayashi, S., Aino, M., Ohno, T., Iwamura, Y., Kikuchi, T., Hayashi, J., Yamamoto, G., Asakura, M., Mitani, A., 2021. Gelatin methacryloyl–riboflavin (GelMA–RF) hydrogels for bone regeneration. Int. J. Mol. Sci. 22, 1635. https://doi.org/10.3390/ijms22041635.

Grilli, F., Pitton, M., Altomare, L., Farè, S., 2022. Decellularized fennel and dill leaves as possible 3D channel network in GelMA for the development of an in vitro adipose tissue model. Front. Bioeng. Biotechnol. 10, 984805 https://doi.org/10.3389/fbioe.2022.984805.

Hachet, E., Van Den Berghe, H., Bayma, E., Block, M.R., Auzély-Velty, R., 2012. Design of biomimetic cell-interactive substrates using hyaluronic acid hydrogels with tunable mechanical properties. Biomacromolecules 13, 1818–1827. https://doi.org/10.1021/bm300324m.

Hammel, J.H., Bellas, E., 2020. Endothelial cell crosstalk improves browning but hinders white adipocyte maturation in 3D engineered adipose tissue. Integr. Biol. 12, 81–89. https://doi.org/10.1093/intbio/zyaa006.

Hong, B.M., Park, S.A., Park, W.H., 2019. Effect of photoinitiator on chain degradation of hyaluronic acid. Biomater. Res. 23, 21. https://doi.org/10.1186/s40824-019-0170-1.

Horder, H., Guaza Lasheras, M., Grummel, N., Nadernezhad, A., Herbig, J., Ergün, S., Teßmar, J., Groll, J., Fabry, B., Bauer-Kreisel, P., Blunk, T., 2021. Bioprinting and differentiation of adipose-derived stromal cell spheroids for a 3D breast cancer-adipose tissue model. Cells 10, 803. https://doi.org/10.3390/cells10040803.

Hou, G., Sun, T., Qian, J., Zhang, Y., Guo, M., Xu, W., Wang, J., Suo, A., 2021. Hydroxyethyl chitosan hydrogels for enhancing breast cancer cell tumorigenesis. Int. J. Biol. Macromol. 184, 768–775. https://doi.org/10.1016/j.ijbiomac.2021.06.110.

Hu, W., Wang, Z., Xiao, Y., Zhang, S., Wang, J., 2019. Advances in crosslinking strategies of biomedical hydrogels. Biomater. Sci. 7, 843–855. https://doi.org/10.1039/C8BM01246F.

Huerta-Reyes, M., Aguilar-Rojas, A., 2021. Three-dimensional models to study breast cancer (Review). Int. J. Oncol. 58, 331–343. https://doi.org/10.3892/ijo.2021.5176.

Janmaleki, M., Liu, J., Kamkar, M., Azarmanesh, M., Sundararaj, U., Nezhad, A.S., 2021. Role of temperature on bio-printability of gelatin methacryloyl bioink in two-step cross-linking strategy for tissue engineering applications. Biomed. Mater. 16, 015021 https://doi.org/10.1088/1748-605X/abbcc9.

Jeon, E.Y., Joo, K.I., Cha, H.J., 2020. Body temperature-activated protein-based injectable adhesive hydrogel incorporated with decellularized adipose extracellular matrix for tissue-specific regenerative stem cell therapy. Acta Biomater. 114, 244–255. https://doi.org/10.1016/j.actbio.2020.07.033.

Karoichan, A., Baudequin, T., Al-Jallad, H., Tabrizian, M., 2022. Encapsulation and differentiation of adipose-derived mesenchymal stem cells in a biomimetic purine cross-linked chitosan sponge. J. Biomed. Mater. Res. 110, 585–594. https://doi.org/10.1002/jbm.a.37311.

Karousou, E., D'Angelo, M.L., Kouvidi, K., Vigetti, D., Viola, M., Nikitovic, D., De Luca, G., Passi, A., 2014. Collagen VI and hyaluronan: the common role in breast cancer. BioMed Res. Int. 2014, 1–10. https://doi.org/10.1155/2014/606458.

Khalighi, S., Saadatmand, M., 2021. Bioprinting a thick and cell-laden partially oxidized alginate-gelatin scaffold with embedded micro-channels as future soft tissue platform. Int. J. Biol. Macromol. 193, 2153–2164. https://doi.org/10.1016/j.ijbiomac.2021.11.046.

Khanmohammadi, M., Nemati, S., Ai, J., Khademi, F., 2019. Multipotency expression of human adipose stem cells in filament-like alginate and gelatin derivative hydrogel fabricated through visible light-initiated crosslinking. Mater. Sci. Eng. C 103, 109808. https://doi.org/10.1016/j.msec.2019.109808.

Kim, H., Kang, B., Cui, X., Lee, S., Lee, K., Cho, D., Hwang, W., Woodfield, T.B.F., Lim, K. S., Jang, J., 2021. Light-activated decellularized extracellular matrix-based bioinks for volumetric tissue analogs at the centimeter scale. Adv. Funct. Mater. 31, 2011252 https://doi.org/10.1002/adfm.202011252.

Kothari, C., Diorio, C., Durocher, F., 2020. The importance of breast adipose tissue in breast cancer. Int. J. Mol. Sci. 21, 5760. https://doi.org/10.3390/ijms21165760.

Kraus, N.A., Ehebauer, F., Zapp, B., Rudolphi, B., Kraus, B.J., Kraus, D., 2016. Quantitative assessment of adipocyte differentiation in cell culture. Adipocyte 5, 351–358. https://doi.org/10.1080/21623945.2016.1240137.

Kumar, H., Sakthivel, K., Mohamed, M.G.A., Boras, E., Shin, S.R., Kim, K., 2021. Designing gelatin methacryloyl (GelMA)-Based bioinks for visible light stereolithographic 3D biofabrication. Macromol. Biosci. 21, 2000317 https://doi.org/10.1002/mabi.202000317.

Lee, S., Lee, H.S., Chung, J.J., Kim, S.H., Park, J.W., Lee, K., Jung, Y., 2021. Enhanced regeneration of vascularized adipose tissue with dual 3D-printed elastic polymer/dECM hydrogel complex. Int. J. Mol. Sci. 22, 2886. https://doi.org/10.3390/ijms22062886.

Li, A., Muenst, S., Hoffman, J., Starck, L., Sarem, M., Fischer, A., Hutter, G., Shastri, V.P., 2022. Mesenchymal-endothelial nexus in breast cancer spheroids induces vasculogenesis and local invasion in a CAM model. Commun. Biol. 5, 1303. https://doi.org/10.1038/s42003-022-04236-5.

Li, C., Ge, J., Guo, Q., Wang, J., Wu, J., Yan, Z., Špitalský, Z., Liu, Y., 2024. Polyvinyl alcohol/collagen composite scaffold reinforced with biodegradable polyesters/gelatin nanofibers for adipose tissue engineering. Int. J. Biol. Macromol. 263, 130237 https://doi.org/10.1016/j.ijbiomac.2024.130237.

Li, S., Poche, J.N., Liu, Y., Scherr, T., McCann, J., Forghani, A., Smoak, M., Muir, M., Berntsen, L., Chen, C., Ravnic, D.J., Gimble, J., Hayes, D.J., 2018. Hybrid synthetic-biological hydrogel system for adipose tissue regeneration. Macromol. Biosci. 18, 1800122 https://doi.org/10.1002/mabi.201800122.

Lim, K.S., Abinzano, F., Bernal, P.N., Albillos Sanchez, A., Atienza-Roca, P., Otto, I.A., Peiffer, Q.C., Matsusaki, M., Woodfield, T.B.F., Malda, J., Levato, R., 2020. One-step photoactivation of a dual-functionalized bioink as cell carrier and cartilage-binding glue for chondral regeneration. Adv. Healthcare Mater. 9, 1901792 https://doi.org/10.1002/adhm.201901792.

Lim, K.S., Klotz, B.J., Lindberg, G.C.J., Melchels, F.P.W., Hooper, G.J., Malda, J., Gawlitta, D., Woodfield, T.B.F., 2019. Visible light cross-linking of gelatin hydrogels offers an enhanced cell microenvironment with improved light penetration depth. Macromol. Biosci. 19, 1900098 https://doi.org/10.1002/mabi.201900098.

Loebel, C., Rodell, C.B., Chen, M.H., Burdick, J.A., 2017. Shear-thinning and self-healing hydrogels as injectable therapeutics and for 3D-printing. Nat. Protoc. 12, 1521–1541. https://doi.org/10.1038/nprot.2017.053.

Louis, F., Pannetier, P., Souguir, Z., Le Cerf, D., Valet, P., Vannier, J., Vidal, G., Demange, E., 2017. A biomimetic hydrogel functionalized with adipose ECM components as a microenvironment for the 3D culture of human and murine adipocytes. Biotechnol. Bioeng. 114, 1813–1824. https://doi.org/10.1002/bit.26306.

Lugo-Cintrón, K.M., Ayuso, J.M., White, B.R., Harari, P.M., Ponik, S.M., Beebe, D.J., Gong, M.M., Virumbrales-Muñoz, M., 2020. Matrix density drives 3D organotypic lymphatic vessel activation in a microfluidic model of the breast tumor microenvironment. Lab Chip 20, 1586–1600. https://doi.org/10.1039/D0LC00099J.

Mehrabi, A., Mousazadeh, S., Mollafilabi, A., Nafissi, N., Milan, P.B., 2023. Synthesis and characterization of a silk fibroin/placenta matrix hydrogel for breast reconstruction. Life Sci. 334, 122236 https://doi.org/10.1016/j.lfs.2023.122236.

Moghanian, A., Portillo-Lara, R., Shirzaei Sani, E., Konisky, H., Bassir, S.H., Annabi, N., 2020. Synthesis and characterization of osteoinductive visible light-activated adhesive composites with antimicrobial properties. J. Tissue Eng. Regen. Med. 14, 66–81. https://doi.org/10.1002/term.2964.

Moon, S.H., Hwang, H.J., Jeon, H.R., Park, S.J., Bae, I.S., Yang, Y.J., 2023. Photocrosslinkable natural polymers in tissue engineering. Front. Bioeng. Biotechnol. 11, 1127757 https://doi.org/10.3389/fbioe.2023.1127757.

Nedunchezian, S., Wu, C.-W., Wu, S.-C., Chen, C.-H., Chang, J.-K., Wang, C.-K., 2022. Characteristic and chondrogenic differentiation analysis of hybrid hydrogels comprised of hyaluronic acid methacryloyl (HAMA), gelatin methacryloyl (GelMA), and the acrylate-functionalized nano-silica crosslinker. Polymers 14, 2003. https://doi.org/10.3390/polym14102003.

Ni, R., Luo, C., Ci, H., Sun, D., An, R., Wang, Z., Yang, J., Li, Y., Sun, J., 2023. Construction of vascularized tissue-engineered breast with dual angiogenic and adipogenic micro-tissues. Mater. Today Bio 18, 100539. https://doi.org/10.1016/j.mtbio.2022.100539.

Paek, K., Woo, S., Song, S.J., Kim, M.K., Yi, K., Chung, S., Kim, J.A., 2024. A well plate-based GelMA photo-crosslinking system with tunable hydrogel mechanical properties to regulate the PTH-mediated osteogenic fate. Biofabrication 16, 025022. https://doi.org/10.1088/1758-5090/ad2a7e.

Paré, M., Darini, C.Y., Yao, X., Chignon-Sicard, B., Rekima, S., Lachambre, S., Virolle, V., Aguilar-Mahecha, A., Basik, M., Dani, C., Ladoux, A., 2020. Breast cancer mammospheres secrete Adrenomedullin to induce lipolysis and browning of adjacent adipocytes. BMC Cancer 20, 784. https://doi.org/10.1186/s12885-020-07273-7.

Pepelanova, I., Kruppa, K., Scheper, T., Lavrentieva, A., 2018. Gelatin-Methacryloyl (GelMA) hydrogels with defined degree of functionalization as a versatile toolkit for 3D cell culture and extrusion bioprinting. Bioengineering 5, 55. https://doi.org/10.3390/bioengineering5030055.

Ruiz-Ojeda, Méndez-Gutiérrez, Aguilera, Plaza-Díaz, 2019. Extracellular matrix remodeling of adipose tissue in obesity and metabolic diseases. Int. J. Mol. Sci. 20, 4888. https://doi.org/10.3390/ijms20194888.

Sakr, M.A., Sakthivel, K., Hossain, T., Shin, S.R., Siddiqua, S., Kim, J., Kim, K., 2022. Recent trends in gelatin methacryloyl nanocomposite hydrogels for tissue engineering. J. Biomed. Mater. Res. 110, 708–724. https://doi.org/10.1002/jbm.a.37310.

Sonbol, H., 2018. Extracellular matrix remodeling in human disease. J. Microsc. Ultrastruct. 6, 123. https://doi.org/10.4103/JMAU.JMAU_4_18.

Teixeira, A.M., Martins, P., 2023. A review of bioengineering techniques applied to breast tissue: mechanical properties, tissue engineering and finite element analysis. Front. Bioeng. Biotechnol. 11, 1161815 https://doi.org/10.3389/fbioe.2023.1161815.

Tytgat, L., Van Damme, L., Ortega Arevalo, M., del, P., Declercq, H., Thienpont, H., Otteveare, H., Blondeel, P., Dubruel, P., Van Vlierberghe, S., 2019. Extrusion-based 3D printing of photo-crosslinkable gelatin and κ-carrageenan hydrogel blends for adipose tissue regeneration. Int. J. Biol. Macromol. 140, 929–938. https://doi.org/10.1016/j.ijbiomac.2019.08.124.

Van Damme, L., Van Hoorick, J., Blondeel, P., Van Vlierberghe, S., 2021. Toward adipose tissue engineering using thiol-norbornene photo-crosslinkable gelatin hydrogels. Biomacromolecules 22, 2408–2418. https://doi.org/10.1021/acs.biomac.1c00189.

Van Den Bulcke, A.I., Bogdanov, B., De Rooze, N., Schacht, E.H., Cornelissen, M., Berghmans, H., 2000. Structural and rheological properties of methacrylamide modified gelatin hydrogels. Biomacromolecules 1, 31–38. https://doi.org/10.1021/bm990017d.

Velasco-Rodriguez, B., Diaz-Vidal, T., Rosales-Rivera, L.C., García-González, C.A., Alvarez-Lorenzo, C., Al-Modlej, A., Domínguez-Arca, V., Prieto, G., Barbosa, S., Soltero Martínez, J.F.A., Taboada, P., 2021. Hybrid methacrylated gelatin and hyaluronic acid hydrogel scaffolds. Preparation and systematic characterization for prospective tissue engineering applications. Int. J. Mol. Sci. 22, 6758. https://doi.org/10.3390/ijms22136758.

Walker, C., Mojares, E., Del Río Hernández, A., 2018. Role of extracellular matrix in development and cancer progression. Int. J. Mol. Sci. 19, 3028. https://doi.org/10.3390/ijms19103028.

Wang, Y., Mirza, S., Wu, S., Zeng, J., Shi, W., Band, H., Band, V., Duan, B., 2018. 3D hydrogel breast cancer models for studying the effects of hypoxia on epithelial to mesenchymal transition. Oncotarget 9, 32191–32203. https://doi.org/10.18632/oncotarget.25891.

Wenz, A., Tjoeng, I., Schneider, I., Kluger, P.J., Borchers, K., 2018. Improved vasculogenesis and bone matrix formation through coculture of endothelial cells and stem cells in tissue-specific methacryloyl gelatin-based hydrogels. Biotechnol. Bioeng. 115, 2643–2653. https://doi.org/10.1002/bit.26792.

Xu, S., Xu, H., Wang, W., Li, S., Li, H., Li, T., Zhang, W., Yu, X., Liu, L., 2019. The role of collagen in cancer: from bench to bedside. J. Transl. Med. 17, 309. https://doi.org/10.1186/s12967-019-2058-1.

Yang, X., Li, X., Wu, Z., Cao, L., 2023. Photocrosslinked methacrylated natural macromolecular hydrogels for tissue engineering: a review. Int. J. Biol. Macromol. 246, 125570 https://doi.org/10.1016/j.ijbiomac.2023.125570.

Young, A.T., White, O.C., Daniele, M.A., 2020. Rheological properties of coordinated physical gelation and chemical crosslinking in gelatin methacryloyl (GelMA) hydrogels. Macromol. Biosci. 20, 2000183 https://doi.org/10.1002/mabi.202000183.

Yue, X., Nguyen, T.D., Zellmer, V., Zhang, S., Zorlutuna, P., 2018. Stromal cell-laden 3D hydrogel microwell arrays as tumor microenvironment model for studying stiffness dependent stromal cell-cancer interactions. Biomaterials 170, 37–48. https://doi.org/10.1016/j.biomaterials.2018.04.001.

Zhang, J., Zeng, Z., Chen, Y., Deng, L., Zhang, Y., Que, Y., Jiao, Y., Chang, J., Dong, Z., Yang, C., 2023. 3D-printed GelMA/CaSiO3 composite hydrogel scaffold for vascularized adipose tissue restoration. Regen. Biomater. 10, rbad049 https://doi.org/10.1093/rb/rbad049.

Zhu, M., Wang, Y., Ferracci, G., Zheng, J., Cho, N.-J., Lee, B.H., 2019a. Gelatin methacryloyl and its hydrogels with an exceptional degree of controllability and batch-to-batch consistency. Sci. Rep. 9, 6863. https://doi.org/10.1038/s41598-019-42186-x.

Zhu, Y., Kruglikov, I.L., Akgul, Y., Scherer, P.E., 2019b. Hyaluronan in adipogenesis, adipose tissue physiology and systemic metabolism. Matrix Biol. 78–79, 284–291. https://doi.org/10.1016/j.matbio.2018.02.012.